RSC Advances

PAPER

View Article Online
View Journal | View Issue

Cite this: *RSC Adv.*, 2020, **10**, 25864

A lauric acid-hybridized bentonite composite phase-changing material for thermal energy storage†

Songyang Liu, *[ab] Jie Han,[ab] Lunan Wang,[ab] Ying Gao,[c] Hai Sun[ab] and Weilong Li[a]

Received 5th September 2019
Accepted 23rd June 2020

DOI: 10.1039/c9ra06936d

rsc.li/rsc-advances

In this study, a form-stable composite phase-changing material (PCM) was synthesised by a vacuum impregnation method. Natural Na-bentonite and lauric acid (LA) were used as the supporting material and PCM, respectively. In addition, flake graphite (FG) was used for enhancing the thermal conductivity of the form-stable composite PCM, besides for blocking the leakage of the PCM. Notably, with the addition of FG, the period of melting and freezing of the composite PCM decreased to a certain extend. Meanwhile, the heat-transfer characteristic of the composite increased. Moreover, the as-prepared form-stable composite PCM showed good thermal reliability after 200 cycles of thermal-cold treatment and has the potential to be used in thermal energy storage systems.

1. Introduction

Nowadays, as many countries are trying to speed up their economic development, conventional energy sources are on the verge of exhaustion. Meanwhile, because of the increase in pollution and the depletion of conventional energy sources, the demand for renewable energy has become increasingly urgent.[1–4] Thermal-energy-storage systems can effectively solve the contradicting problems of energy source shortage and environmental pollution.[5–7] They can also increase the efficiency of energy utilization. Compared with the sensitive heat-storage and other energy-storage systems, latent heat storage systems play an important role in the energy structure because of their higher energy density and minor temperature fluctuation.[8–11]

At present, as a new type of recyclable energy-storage materials, phase-changing material (PCM), is being most commonly applied in latent heat storage systems because of their high heat-storage capacity and stable phase-change temperature.[12–14] Moreover, during phase transition, PCMs store and release latent heat in a steady-state, which can be widely used for saving energy in buildings, and in concentrated solar energy utilization and waste heat recovery systems.[15] Different kinds of PCMs, including inorganic, organic and their mixtures, have been investigated as PCMs in latent-heat-storage system.[16–18] Among the studied PCMs, fatty acids have become increasingly important in the field of energy-saving buildings, passive solar energy storage and industrial waste heat recovery systems due to their relatively low supercooling temperatures, a wide range of service temperatures and stable chemical and thermal properties after long-term usage.[19,20] However, two main drawbacks of fatty acids restrict their application in many fields. One is the characteristic of low thermal conductivity, which does not satisfy the requirement for thermal energy storage systems, and the other is the leakage problem during utilization.[21,22]

Most of the clay mineral materials have a peculiar structure and surface property, which can be used to support PCMs. Based on the compressible skeleton of the clay mineral materials, the heat-conducting capabilities of the composite PCMs can be improved to some extent. Moreover, the surface tension and capillary action in the pores of the clay mineral materials can be used to solve the leakage problem and form a shape-stabilized state. Clay mineral materials, such as kaolin,[23–25] diatomite,[26–28] sepiolite,[29] attapulgiate[30,31] and expanded perlite[32,33] have also been employed as supporting matrices. Bentonite has a multi-layer structure, and it is a common industrial clay, such as the clay minerals of the smectite group. For its good physical and chemical properties, bentonite is broadly used as a functional filler, binder, thixotropic agent and catalyst. In addition, bentonite has the advantages of good chemical and thermal stability, excellent adsorption characteristics, and low price, which make it suitable for the synthesis of form-stable composite PCMs.

In this work, a novel composite PCM made of LA/Na-bentonite-1 with high latent heat storage capacity and an appropriate phase-change temperature for energy-saving systems were prepared by a vacuum impregnation method. Natural bentonite and LA were used as the supporting material

[a]School of Civil Engineering, Liaoning Shihua University, Fushun 113001, China. E-mail: liusongyanglnsh@163.com; Tel: +86-24-56863306

[b]Liaoning Key Lab of Petro-chemical Special Building Materials, Liaoning Shihua University, Fushun 113001, China

[c]School of Chemistry and Materials Science, Liaoning Shihua University, Fushun 113001, China

† Electronic supplementary information (ESI) available. See DOI: 10.1039/c9ra06936d

and PCM, respectively. Furthermore, it was found that a suitable portion of FG could not only improve the thermal conductivity of the composite PCM, but also prevent LA leakage from the composite PCM. The prepared form-stable composite PCM showed good performance with thermal reliability after 200 heating–cooling treatment cycles and has the potential to be used in thermal-energy-storage systems.

2. Experimental methods

2.1 Materials

The raw bentonite used was unmodified Na-bentonite from Shandong, Jining, China. The main chemical composition of bentonite included (wt%): SiO_2 (66.8), Al_2O_3 (15.8), Fe_2O_3 (7.6), CaO (3.9), K_2O (2.0), MgO (1.2), and P_2O_5 (0.9). It was passed through a 74 μm sieve and dried at 105 °C for 24 h before use. Lauric acid (LA) was purchased from Sinopharm Chemical Reagent Co., Ltd. Natural FG (99%, lateral size 0.5–1.0 mm and thickness 0.01–0.03 mm) was supplied by Qingdao Tengshengda Carbon Co., Ltd., China. The pore size distribution and particle size distribution of Na-bentonite were studied using the Barrett–Joyner–Halenda (BJH) method and a particle size analyzer, respectively.

2.2 Characterization

The structural and chemical compatibility of Na-bentonite, LA, FG and the bentonite-based composite PCMs were investigated by X-ray diffraction (XRD) and Fourier transform infrared spectroscopy (FTIR). The XRD analysis of the samples was carried out using an X-ray diffraction apparatus (DX-2700) using Cu Kα radiation ($\lambda = 1.5418$ Å) with an acceleration voltage of 40 kV and an emission current of 40 mA at a scanning rate of 9° min^{-1} in the 2θ range of 5° to 60°. The FTIR spectra were recorded on a Nicolet 5700 spectrophotometer. The morphology of Na-bentonite, FG and bentonite-based composite PCMs were observed using scanning electron microscopy (SEM), which was performed with a field-emission scanning electron microscope (TESCAN, Model MIRA3 LMU) system after coating the samples were with conductive gold. The scanning transmission electron microscopy (STEM) images of LA/Na-bentonite and LA/Na-bentonite-1 were collected on a JEOL JEM-2100F electron microscope. Autosorb-IQ2-MP was used to test the Brunauer–Emmett–Teller (BET) surface area and the pore size characteristics of the samples. Malvern Mastersizer was used to test the particle size distributions of the samples. The photomicrographs of the samples were obtained using an Olympus BX51 photomicroscope.

The phase-changing properties of LA and the bentonite-based composite PCMs were studied on a differential scanning calorimeter (DSC Q10, TA instruments). A thermogravimetric analyser (TGA) Q600 was used to investigate the maximum load of the composite PCM and thermal stability from room temperature to 800 °C at 10 °C min^{-1} under N_2 flow. The thermal storage and release performance of the PCM and composite PCMs were studied by self-assembled equipment. First, the test tubes with the samples were placed in a water bath (30 °C) until the temperature reached the set temperature (80 °C). Afterwards, the test tubes were placed in the thermostatic water bath (30 °C). A thermocouple was used to record the temperature variations in the composite PCMs at time intervals of 10 s. The cycling performance of LA/Na-bentonite-1 was assessed over 200 cycles to study the thermal reliability after long-time utilization. The thermal conductivities of the samples were recorded on a thermal constants analyzer (TC 3100).

2.3 Preparation of phase-change bentonite

LA/Na-bentonite was prepared by a vacuum impregnation method. First, 30 g of Na-bentonite and 70 g of LA were added into a reaction vessel, which was linked to a vacuum pump through a backflow prevention device. The reaction vessel containing the mixture of Na-bentonite and LA was stirred at a constant-temperature bath at 80 °C for 45 min and then mixed using ultrasound under the pressure of 0.1 MPa until the mixture was homogeneous. After cooling, the sample was placed in an automatic electric oven at 80 °C for 24 h to remove superfluous LA, and the composite was named LA/Na-bentonite. LA/Na-bentonite-1 was also synthesized by the vacuum impregnation method. 30 g of Na-bentonite, 70 g of LA and 5 g FG were added into the reaction vessel. The preparation process was the same as that employed for LA/Na-bentonite. Finally, the composite obtained was named LA/Na-bentonite-1.

In order to further study the function of FG on the phase change behaviors of the composite PCMs, natural FG was mixed homogeneously with Na-bentonite and LA at different mass fractions: 8 wt% and 11 wt% (named as LA/Na-bentonite-2 and LA/Na-bentonite-3, respectively). For these LA/Na-bentonite/FG composites, prior to pouring the LA/Na-bentonite solution into a glass beaker, different ratios of FG (8 wt% and 11 wt%) were added and stirred with a magnetic stirrer for 45 min at 700 rpm, and the heating temperature was maintained at 80 °C. The subsequent preparation process was the same as that used for LA/Na-bentonite-1. We could see no significant difference in the phase change temperature and the latent heat capacity of the bentonite-based composite PCMs with increasing FG content (Table 1). In addition, the economics of the novel composite PCMs were further investigated, being natural minerals, bentonite only cost 100 USD per ton, LA cost 800 USD per ton and FG cost 300 USD per ton. Therefore, the cost of the hybrid bentonite-based phase change materials increases with the amount of FG added. Therefore, since there were no changes in the phase change behaviors, 5 wt% of FG was added, and LA/Na-bentonite-1 was used as the main sample for investigation.

3. Results and discussion

3.1 Characterization of the Na-bentonite

While investigating the promising PCM candidates, we considered the leakage problem, as well as to the main features of the porous network, such as porosity, particle size and distribution in the matrix. Fig. 1a shows the photo of natural Na-bentonite. The particle size and distribution of Na-bentonite

Table 1 Thermal properties of lauric acid and the bentonite-based composites

Samples	Melting temperature (T_m, °C)	Freezing temperature (T_f, °C)	Latent heat of melting (J g^{-1})	Latent heat of freezing (J g^{-1})
Pure LA	42.28	44.03	175.6	172.8
LA/Na-bentonite	42.03	43.58	114.3	111.3
LA/Na-bentonite-1	41.97	43.33	113.7	109.6
LA/Na-bentonite-2	41.76	43.12	112.9	108.8
LA/Na-bentonite-3	41.65	43.01	111.7	107.9

were studied by the dynamic scattering of the laser light. Fig. 1b demonstrates that the average particle diameter ($d_{0.5}$) of Na-bentonite was 16.75 μm. The N_2 adsorption–desorption isotherms and the corresponding pore size distribution curve of Na-bentonite are shown in Fig. 1c and d, respectively. It showed a type IV isotherm with a hysteresis loop characteristic, which is typical of mesoporous solids. The BET surface area (S_{BET}) and the total pore volumes were 98.7 m^2 g^{-1} and 0.06 cm^3 g^{-1}, respectively.

3.2 XRD and FTIR characterization of the composite PCMs

Fig. S1a† shows the XRD patterns of Na-bentonite, LA, LA/Na-bentonite, FG and LA/Na-bentonite-1. It can be seen that montmorillonite ($2\theta = 6.8°$, 12.3° and 19.8°) and quartz ($2\theta = 20.8°$, 26.6°) were the major phases of Na-bentonite. Pristine LA had four main diffraction peaks at $2\theta = 19.2°$, $2\theta = 19.8°$, $2\theta = 23.4°$ and $2\theta = 24.3°$. All the reflections of Na-bentonite and LA appeared in the pattern of the LA/Na-bentonite composite, which manifested that LA was successfully impregnated into Na-bentonite. FG displayed a strong diffraction peak at $2\theta = 26.5°$ and another weaker peak at $2\theta = 54.7°$ for the (002) and (004) planes of the graphite layers, which is in agreement with the previous reports.[34] In the spectra of the LA/Na-bentonite and LA/Na-bentonite-1 composites, the diffraction peak for LA could be observed, and certain easily-detectable peaks were mainly rooted in the crystallinity of the bentonite-based constituent.

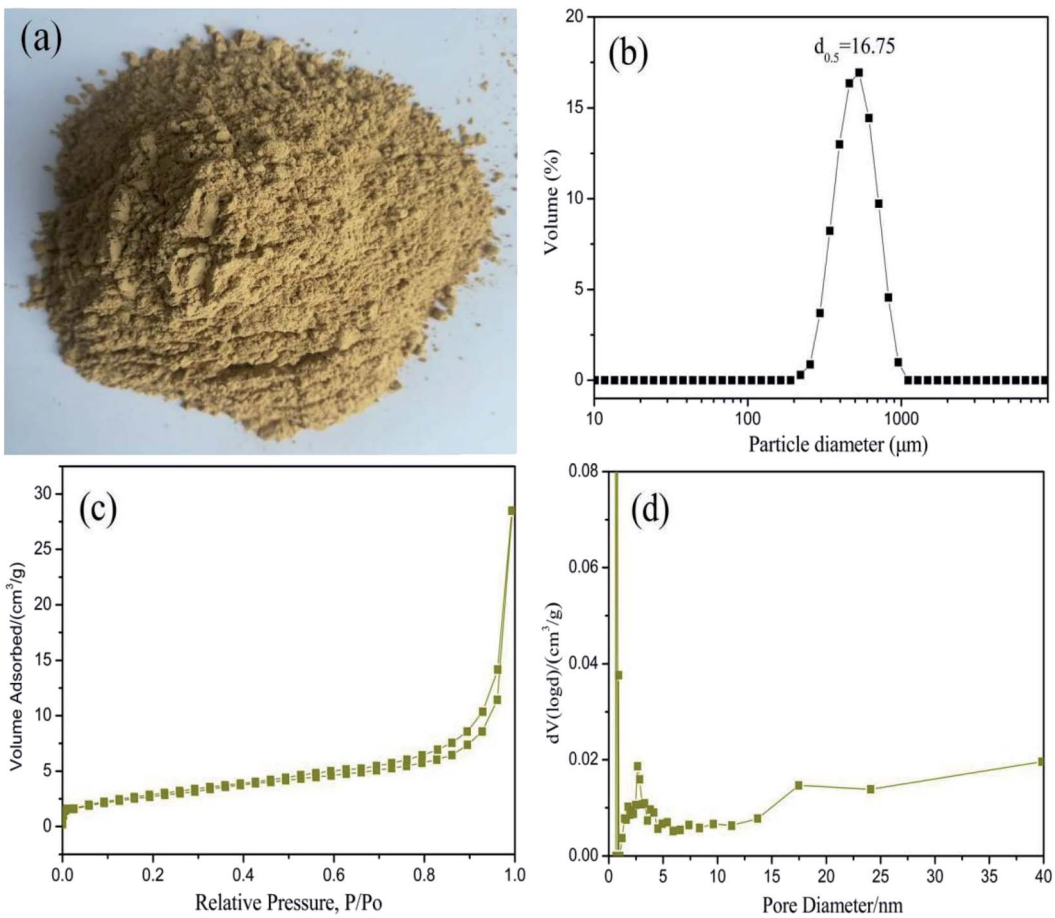

Fig. 1 (a) Photograph, (b) particle size distribution, (c) particle size distribution isotherms and (d) BJH pore size distribution of Na-bentonite.

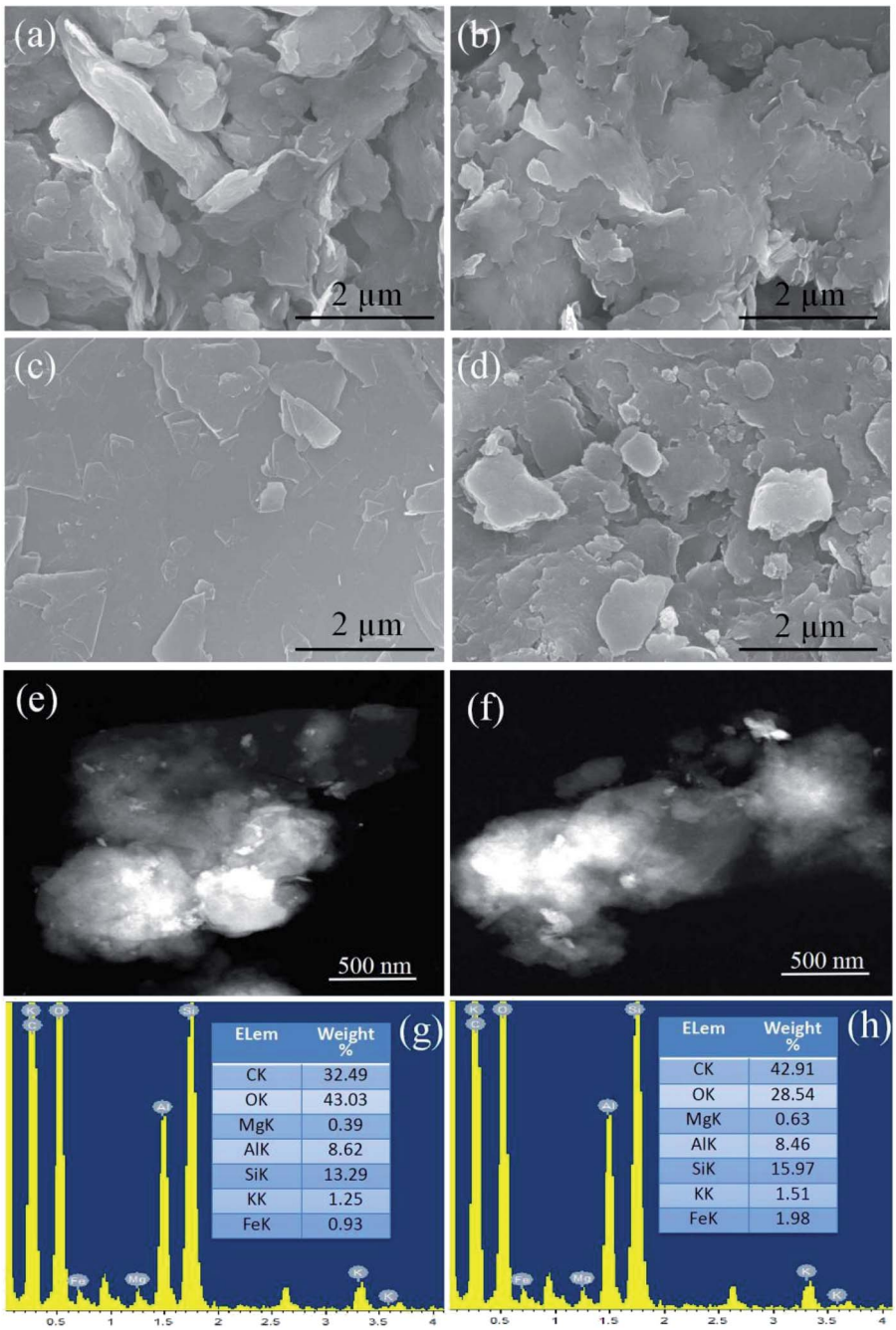

Fig. 2 SEM images of (a) Na-bentonite, (b) LA/Na-bentonite, (c) FG, and (d) LA/Na-bentonite-1; STEM images of (e) LA/Na-bentonite and (f) LA/Na-bentonite-1; EDS spectra and the corresponding elemental composition of (g) LA/Na-bentonite and (h) LA/Na-bentonite-1.

No other diffraction peaks were recorded in the XRD patterns of the composites, which meant that there had been no chemical reaction between the supports and LA during the whole impregnation process. Furthermore, it was remarkable that the relative intensity of LA reflections in the LA/Na-bentonite-1 composite was higher than that in the LA/Na-bentonite composite, drawing that the layer thickness of the LA/Na-bentonite-1 composite increased with the addition of FG. This is due to the XRD diffraction occurring between the atoms of different layers instead of the atoms at the same layer, so that the greater the layer number, the higher would be the peak intensity. Fig. S1b† illustrates the FTIR spectra of Na-bentonite, LA, LA/Na-bentonite, FG and LA/Na-bentonite-1. In the FTIR spectrum of Na-bentonite, the peaks at 3617 cm^{-1} and 1637 cm^{-1} were due to the stretching and bending vibrations arising from water molecules in the structure of Na-bentonite, and the peak at 1043 cm^{-1} denoted the Si–O–Si antisymmetric vibration. The absorption peaks at 2953 cm^{-1} and 2917 cm^{-1} in the spectrum of pure LA signified the asymmetrical and symmetrical stretching vibrations of the $-CH_3$ group.

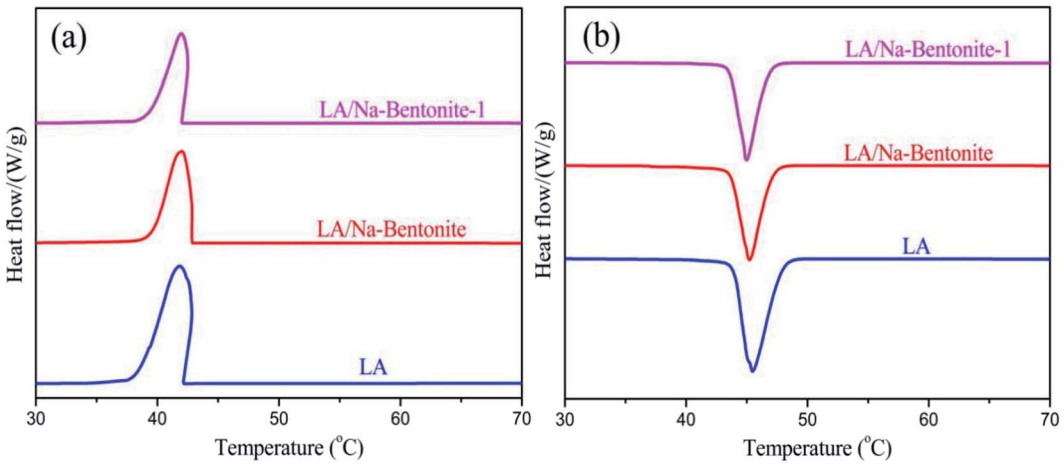

Fig. 3 DSC thermograms of LA, LA/Na-bentonite and LA/Na-bentonite-1 in the (a) melting cycles and (b) freezing cycles.

The peak at 2849 cm^{-1} was ascribed to the symmetrical stretching vibration of the $-CH_2$ group. The peak at 1701 cm^{-1} was associated with the C=O stretching vibration, and the characteristic absorption peak at 1303 cm^{-1} represented its bending vibration. Notably, the LA/Na-bentonite spectrum contained all the characteristic peaks of Na-bentonite and pure LA. In the spectrum of FG, the peak at 3447 cm^{-1} was assigned to the stretching vibration of –OH. Moreover, no distinct new absorption peaks appeared in the LA/Na-bentonite-1 spectrum, which manifested that there was no chemical interaction between the supports and LA.

3.3 Morphology and microstructure of the composite PCMs

Fig. 2 shows the morphology of the natural Na-bentonite powder, LA/Na-bentonite, FG and LA/Na-bentonite-1. As shown in Fig. 2a, the lamellar structure of Na-bentonite, which consisted of stacked layers, was clearly observed. We could clearly see that the surface of Na-bentonite was occupied entirely by LA in LA/Na-bentonite after impregnation (Fig. 2b). Moreover, the shape was not stably retained because Na-bentonite was too small for LA to envelop the composite PCM at the melting state. Therefore, the problem of its platelet microstructure absorbing excess LA can be resolved by adding FG proportionally. In Fig. 2c, it can be seen that FG has a comparatively clear and smooth surface without obvious cracks or defects. Fig. 2d shows the composite PCM doped with FG, in which the ratio of Na-bentonite and LA remained unchanged (3 : 7) and the mass fraction of FG was 5 wt%. It can be clearly seen that the platelet structure of the composite had become increasingly obvious. This phenomenon demonstrated that LA/Na-bentonite and FG had mixed together successfully and that the addition of FG could reduce LA leakage from Na-bentonite to some extent. Moreover, the LA/Na-bentonite-1 composite remained shape-stabilized again with the help of FG. Fig. 2e–h shows the STEM images and corresponding energy spectra of LA/Na-bentonite and LA/Na-bentonite-1. It could be clearly seen that LA/Na-bentonite and LA/Na-bentonite-1 had a lamellar structure. Moreover, with the addition of 5 wt% FG, the content of carbon in LA/Na-bentonite-1 increased to some extent, as per the EDS analysis in Fig. 2g and h.

3.4 Phase change behaviour of composite PCMs

Fig. 3 shows the DSC curves of LA, LA/Na-bentonite and LA/Na-bentonite-1 in the melting (Fig. 3a) and freezing (Fig. 3b) processes. Moreover, the data corresponding to the phase change temperature and latent heat of the bentonite-based composite PCMs are listed in Table 1. As shown in Fig. 3

Table 2 Comparison of shape-stabilized composite PCMs in the literature

	Melting		Solidification		
Samples	T_m (°C)	H_m (J g^{-1})	T_s (°C)	H_s (J g^{-1})	Ref.
Capric acid/halloysite nanotube/graphite	29.56	75.4	25.4	75.35	36
Lauric acid/expanded perlite/expanded graphite	44.3	86.7	40.2	86.9	37
Stearic acid/bentonite/graphite	53.36	84.6	52.94	84.1	38
Polyethylene glycols/diatomite/Ag nanoparticles	59.83	110.7	39.54	103.3	39
LA/Na-bentonite-1	41.97	113.7	43.33	109.6	This work

Table 3 Thermal conductivities of the Na-bentonite, LA, FG, LA/Na-bentonite and LA/Na-bentonite-1

Samples	Na-bentonite	LA	FG	LA/Na-bentonite	LA/Na-bentonite-1
λ (W m^{-1} K^{-1})	1.161	0.115	5.438	0.441	0.569

and Table 1, LA melted at 42.28 °C and solidified at 44.03 °C. The latent heat of melting (ΔH_m) and freezing (ΔH_f) of LA were 175.6 J g^{-1} and 172.8 J g^{-1}, respectively. In comparison with LA, the melting temperature (T_m) and freezing temperature (T_f) of LA/Na-bentonite were measured to be 42.03 °C and 43.58 °C, respectively. Moreover, the latent heat values for the melting and freezing of LA/Na-bentonite were 114.3 J g^{-1} and 111.3 J g^{-1}, respectively. It could be seen that LA/Na-bentonite-1 melted at 41.97 °C with a latent heat of 113.7 J g^{-1} and solidified at 43.33 °C with a latent heat of 109.6 J g^{-1} when the maximum load of LA reached 65%. The experimental values were less than the corresponding theoretical values (for the LA/Na-bentonite-1 composite, ΔH_m = 175.6 J g^{-1} × 65% = 114.1 J g^{-1}, ΔH_f = 172.8 J g^{-1} × 65% = 112.3 J g^{-1}). There could be two possible reasons; one is that the crystal arrangement and orientation of the LA molecular chains were limited by the drag and steric effects of the nano and meso-pores, which may cause a reduction in the regularity of the crystalline regions, and the other is the loss of LA during measurement. In addition, we could also clearly see that there was a small decrease in the phase change temperature between LA/Na-bentonite and LA/Na-bentonite-1. The decrease was due to the weak attractive interaction between the inner surface wall of the porous supporting material and the LA molecules.[35] Table 2 shows the comparison of the phase change temperatures and enthalpy values of some typical shape-stabilized composite PCMs in the literature.[36–39] The LA/Na-bentonite-1 demonstrated obvious advantages over these reported materials to some extent. Notably, the prepared LA/Na-bentonite-1 composite can be a preferential solar thermal-energy-storage material for use in the energy-saving systems.

3.5 Thermal conductivity improvement of the composite PCMs

For composite phase-changing materials, thermal conductivity is a crucial parameter in practical applications. It is known that the thermal conductivity of fatty acids is relatively low, and LA is no exception. Therefore, improving thermal conductivity is crucial in the process of designing materials. The thermal conductivity of the composite PCM was enhanced by adding the FG because of its high thermal conductivity (2–90 W m^{-1} K^{-1}). Thus, FG was selected to improve the thermal conductivity of the composite PCM. Table 3 shows the thermal conductivities of Na-bentonite, LA, FG, LA/Na-bentonite and LA/Na-bentonite-1. Pure LA has a low thermal conductivity of 0.115 W m^{-1} K^{-1}

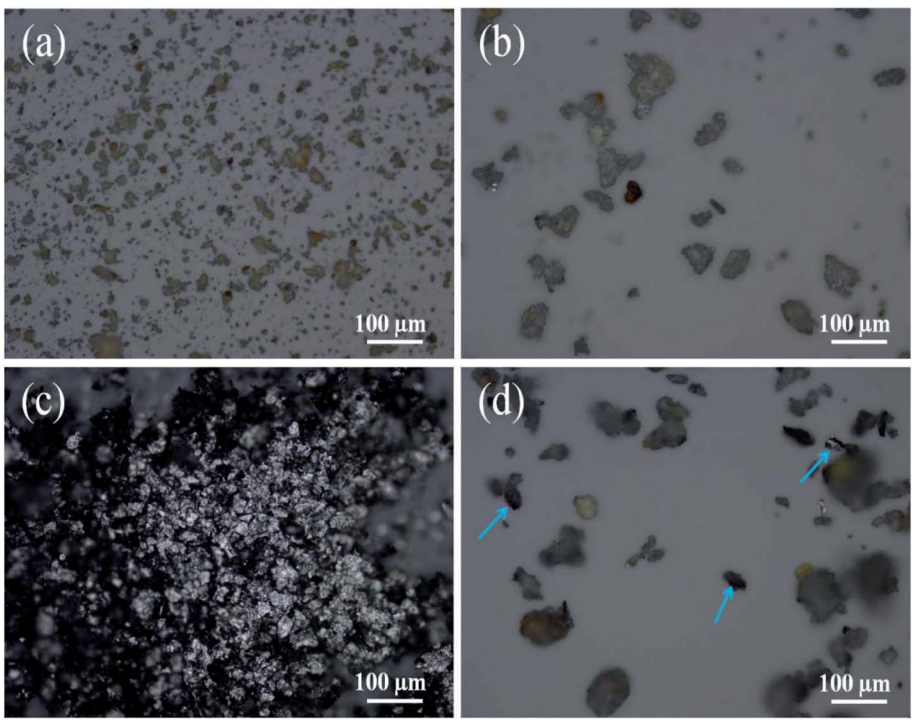

Fig. 4 Photomicrographs of (a) Na-bentonite, (b) LA/Na-bentonite, (c) FG, and (d) LA/Na-bentonite-1.

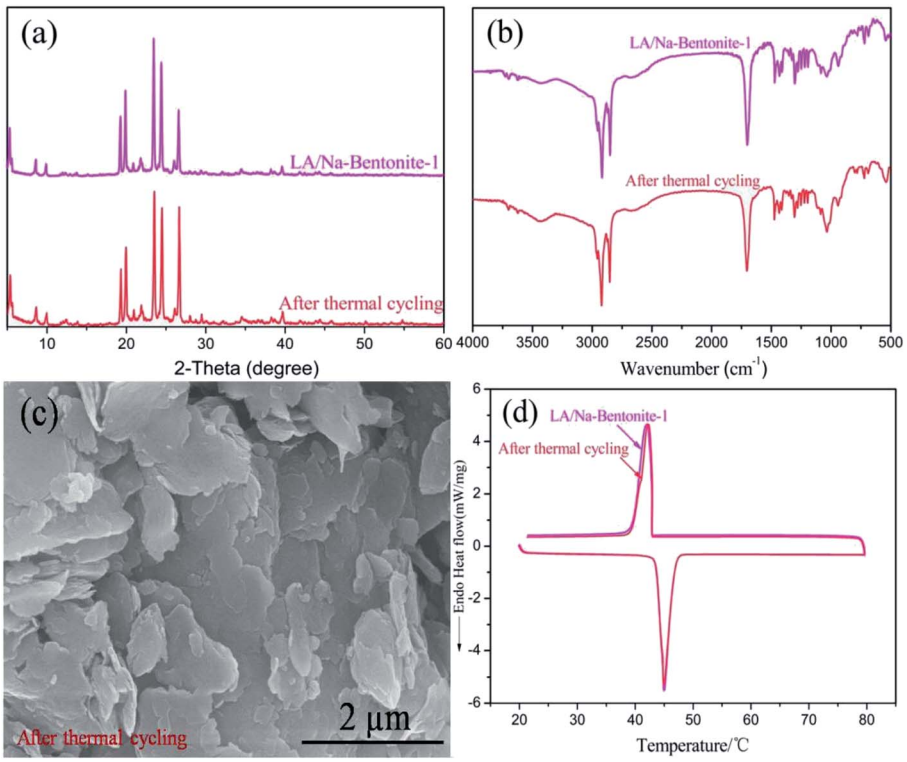

Fig. 5 (a) XRD patterns, (b) FTIR spectra, (c) SEM images and (d) DSC curves of LA/Na-bentonite-1 before and after the thermal cycling treatment.

like other organic PCMs. In the meantime, the thermal conductivity of LA/Na-bentonite and LA/Na-bentonite-1 were measured to be 0.441 and 0.569 W m^{-1} K^{-1}, which are about 3.83 and 4.95 times than those of LA, respectively. The result manifested that the addition of FG enhanced the thermal conductivity of the composite PCMs to some extent.

To further investigate the function of FG in improving the heat transfer of the composite PCM, photomicrographs were used to observe the microstructure and ascertain the state of LA/Na-bentonite and LA/Na-bentonite-1. It can be seen clearly in Fig. 4a that the flake-like particles of Na-bentonite were distributed randomly. After LA impregnation, the particle size of LA/Na-bentonite increased obviously (Fig. 4b). As seen in Fig. 4c, the particle size of FG with a silver-white color distribution was more concentrated than that of the natural Na-bentonite particles. The particles were more closely distributed with the addition of FG, as indicated by the arrow points in Fig. 4d. Beyond that, with the addition of FG, the particles interacted with each other to form an effective heat transfer network structure between LA and the supporting materials. Therefore, the heat transfer performance of LA/Na-bentonite-1 would be improved by the induction of FG.

3.6 Heat storage/release properties of the composite PCMs

The heat storage/release rate can be affected by thermal conductivity to some extent. The improvement in the heat transfer rates of LA/Na-bentonite and LA/Na-bentonite-1 compared with LA during the heating and cooling processes was studied by a self-designed device. Fig. S2† demonstrates the melting and freezing curves of LA, LA/Na-bentonite and LA/Na-bentonite-1. The initial temperature of the heat storage process was 30 °C. We could clearly see that the temperature of LA, LA/Na-bentonite and LA/Na-bentonite-1 gradually increased over time. LA needed 675 s to reach its melting point, whereas only 525 s and 415 s were sufficient for LA/Na-bentonite and LA/Na-bentonite-1, respectively. It was obvious that the thermal storage efficiency of LA/Na-bentonite-1 was much better than those of LA and LA/Na-bentonite. It was difficult for pure LA to reach 80 °C, and it took the longest time (2470 s) to reach the equilibrium temperature (79.4 °C), whereas LA/Na-bentonite

Table 4 Thermal properties of LA/Na-bentonite-1 after 10, 100 and 200 heating–cooling cycles

Cycles	Melting temperature (T_m, °C)	Freezing temperature (T_f, °C)	Latent heat of melting (J g^{-1})	Latent heat of freezing (J g^{-1})
10	41.93	43.31	113.6	109.3
100	41.91	43.29	113.5	109.1
200	41.85	43.22	113.1	108.5

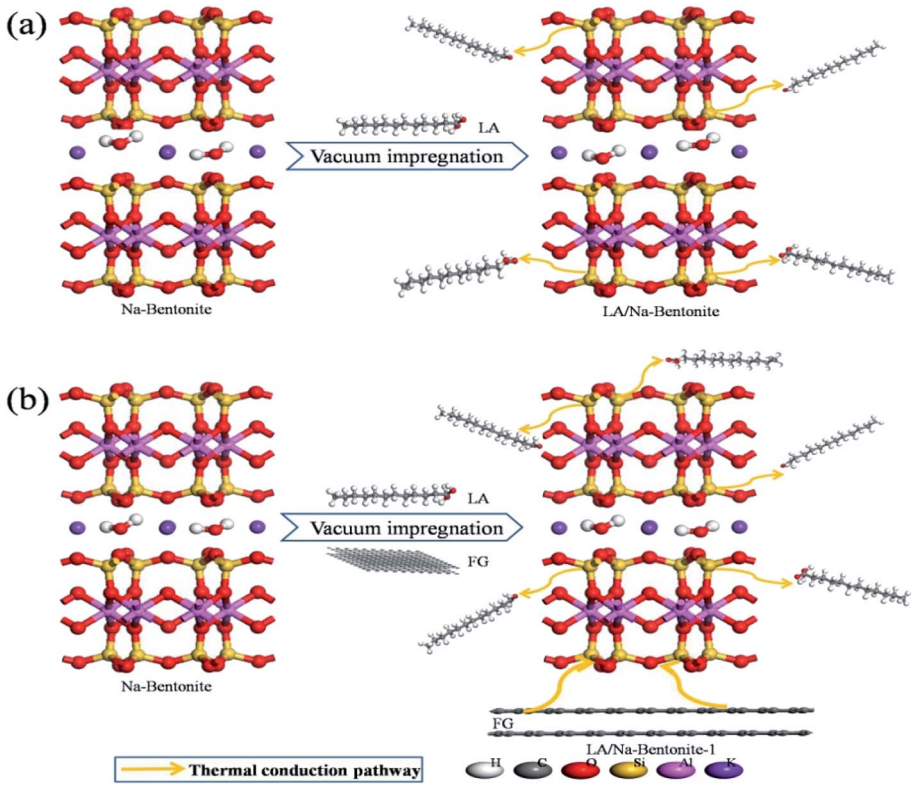

Fig. 6 Schematic illustration for the preparation and improvement of the thermal conduction pathway of (a) LA/Na-bentonite and (b) LA/Na-bentonite-1.

and LA/Na-bentonite-1 took 1995 s and 1605 s, respectively. In the freezing process, it took 1505 s for pure LA to reach the solidifying temperature compared with 1125 s and 1065 s for LA/Na-bentonite and LA/Na-bentonite-1, respectively. The thermal storage/release rates of pure LA were significantly improved by the addition of the supporting materials, according to the above analysis. Compared with LA and LA/Na-bentonite, LA/Na-bentonite-1 showed better thermal storage/release rates. In other words, the addition of FG improved the thermal storage/release rate obviously.

3.7 Thermal reliability of LA/Na-bentonite-1

For form-stable composite PCMs, it is very important to investigate the thermal reliability characteristics over the full operating temperature range after long-time utilization. An experiment with 200 heating–cooling cycles was conducted to study the thermal stability of LA/Na-bentonite-1. Fig. 5a and b show the XRD patterns and the FTIR spectra of LA/Na-bentonite-1 before and after 200 heating–cooling cycles. No obvious variation in the two diffraction peaks was observed after thermal cycling, which meant that the crystal structure of LA/Na-bentonite-1 was not influenced by the thermal cycling treatment (Fig. 5a). Moreover, the characteristic bands of LA/Na-bentonite-1 were also not affected by the heating–cooling cycles, which further proved the structural stability of the composite PCM (Fig. 5b). Fig. 5c shows the SEM images of LA/Na-bentonite-1 after 200 heating–cooling cycles, which indicated that the surface of the composite was also covered by continuous LA. As seen in Fig. 5d, the phase change enthalpy and temperature in the melting and freezing processes of LA/Na-bentonite-1 were 113.1 J g^{-1} at 41.85 °C and 108.5 J g^{-1} at 43.22 °C after 200 thermal cycles, respectively. The phase change enthalpy during the melting and freezing processes had changed by 0.6 J g^{-1} and 1.1 J g^{-1}, and the melting and freezing temperatures of the composite PCM had changed by 0.12 °C and 0.11 °C, respectively.

LA/Na-bentonite-1 was also tested with 10 and 100 heating–cooling cycles to investigate whether the heat-storage capability was conserved during cycling. It can be seen from Table 4 that the LA/Na-bentonite-1 melted at 41.93 °C with an enthalpy of 113.6 J g^{-1} and at 41.91 °C with an enthalpy of 113.5 J g^{-1} after 10 and 100 heating–cooling cycles, respectively. Notably, there was very little change in the phase-changing behaviors of LA/Na-bentonite-1 after 10 and 100 heating–cooling cycles, which proved its good thermal reliability and that it could be potentially used for low-temperature thermal energy storage.

Based on the experimental results and in order to investigate the effect of FG introduction on the heat-transfer characteristics of the bentonite-based composite PCMs, the synthetic process and thermal conduction pathway of LA/Na-bentonite and LA/Na-bentonite-1 are schematically depicted at the atomic level (Fig. 6). The crystal of natural Na-bentonite had a 2:1 layered structure formed by SiO_4 tetrahedral sheets and $AlO_2(OH)_4$ octahedral sheets. Based on the mineral structure of Na-

bentonite and using its porous mineral medium skeleton, we improved the thermal conductivity of the composite PCM. As a result, the cross-linked three-dimensional network of Na-bentonite acted as an efficient pathway for thermal conduction, and the thermal conductivity of LA/Na-bentonite (0.441 W m^{-1} K^{-1}) has higher than that of pure LA (0.115 W m^{-1} K^{-1}). As shown in Fig. 6a, natural Na-bentonite was impregnated with LA by the vacuum impregnation method to prepare LA/Na-bentonite. The adsorption mainly relied on the surface tension and capillary action of the supporting materials. Moreover, we could clearly see that heat flowed from Na-bentonite to LA randomly. It is obvious from Fig. 6b that LA/Na-bentonite-1 contained additional thermal conduction pathways when the highly conductive material (FG with thermal conductivity of 5.438 W m^{-1} K^{-1}) was added. This meant that the addition of FG can provide to more active sites for thermal transfer in LA/Na-bentonite-1.

4. Conclusions

In this work, the shape-stabilized composite LA/Na-bentonite-1 has been successfully prepared through the vacuum impregnation method for thermal energy storage. LA was successfully impregnated into Na-bentonite, and the maximum capacity with good shape stability was reached at 65 wt%. The form-stable phase change material LA/Na-bentonite-1 melted at 41.97 °C with a latent heat of 113.7 J g^{-1} and solidified at 43.33 °C with a latent heat of 109.6 J g^{-1}. Moreover, the addition of FG had a significant effect on the heat-storage/release rate and the thermal conductivity enhancement of the form-stable composite PCM. In conclusion, the novel form-stable PCM optimized with FG had a stable shape, excellent thermal properties and favourable thermal conductivity. It is a promising candidate for application in low-temperature solar energy systems.

Conflicts of interest

There are no conflicts to declare.

Acknowledgements

This work is supported by the Fundamental Research Project of the Educational Department of Liaoning Province (grant no. L2017LQN033 and grant no. L2017LQN034), the Liaoning Key Lab of Petro-chemical Special Building Materials. The authors also wish to thank the reviewers and editor for kindly giving revising suggestions.

Notes and references

1 C. Li, B. Xie, J. Chen, Z. He, Z. Chen and Y. Long, *Energy Convers. Manage.*, 2019, **183**, 633–644.
2 X. Yang, Z. Guo, Y. Liu, L. Jin and Y. He, *Appl. Energy*, 2019, **238**, 22–33.
3 A. Sarı, R. Sharma, G. Hekimoğlu and V. V. Tyagi, *Energy Build.*, 2019, **188–189**, 111–130.
4 F. Tang, D. Su, Y. Tang and G. Fang, *Sol. Energy Mater. Sol. Cells*, 2015, **141**, 218–224.
5 Y. Zhang, J. Wang, J. Qiu, X. Jin, M. M. Umair, R. Lu, S. Zhang and B. Tang, *Appl. Energy*, 2019, **237**, 83–90.
6 H. Yu, J. Gao, Y. Chen and Y. Zhao, *J. Therm. Anal. Calorim.*, 2016, **124**, 87–92.
7 S. Liu and H. Yang, *RSC Adv.*, 2016, **6**, 48033–48042.
8 Y. Deng, J. Li, T. Qian, W. Guan, Y. Li and X. Yin, *Chem. Eng. J.*, 2016, **295**, 427–435.
9 M. M. Umair, Y. Zhang, K. Iqbal, S. Zhang and B. Tang, *Appl. Energy*, 2019, **235**, 846–873.
10 C. Liu, Y. Yuan, N. Zhang, X. Cao and X. Yang, *Mater. Lett.*, 2014, **120**, 43–46.
11 J. Yang, G. Qi, Y. Liu, R. Bao, Z. Liu, W. Yang, B. Xie and M. Yang, *Carbon*, 2016, **100**, 693–702.
12 L. Xia, P. Zhang and R. Wang, *Carbon*, 2010, **48**, 2538–2548.
13 J. Wang, M. Yang, F. Lu, K. Jin, L. Tan, Y. Gao, S. Fan, J. Dong and G. Wang, *Nano Energy*, 2016, **19**, 78–87.
14 C. Li, B. Zhang, B. Xie, X. Zhao and J. Chen, *Energy Convers. Manage.*, 2020, **208**, 112586.
15 C. Li, B. Xie, Z. He, J. Chen and Y. Long, *Renewable Energy*, 2019, **140**, 862–873.
16 D. Kim, J. Jung, Y. Kim, M. Lee, J. Seo and S. B. Khan, *Int. J. Heat Mass Transfer*, 2016, **95**, 735–741.
17 T. Khadiran, M. Z. Hussein, Z. Zainal and R. Rusli, *Renewable Sustainable Energy Rev.*, 2016, **57**, 916–928.
18 A. Karaipekli and A. Sarı, *Sol. Energy Mater. Sol. Cells*, 2016, **149**, 19–28.
19 S. Liu and H. Yang, *Energy Technol.*, 2015, **3**, 77–83.
20 S. Harish, D. Orejon, Y. Takata and M. Kohno, *Appl. Therm. Eng.*, 2015, **80**, 205–211.
21 G. Qi, J. Yang, R. Bao, Z. Liu, W. Yang, B. Xie and M. Yang, *Carbon*, 2015, **88**, 196–205.
22 B. Tang, M. Qiu and S. Zhang, *Sol. Energy Mater. Sol. Cells*, 2012, **105**, 242–248.
23 S. Song, L. Dong, Y. Zhang, S. Chen, Q. Li, Y. Guo, S. Deng, S. Si and C. Xiong, *Energy*, 2014, **76**, 385–389.
24 A. Sarı, *Energy Build.*, 2015, **96**, 193–200.
25 S. Liu, Z. Yan, L. Fu and H. Yang, *Sol. Energy Mater. Sol. Cells*, 2017, **167**, 140–149.
26 A. Miliozzi, M. Chieruzzi and L. Torre, *Appl. Energy*, 2019, **250**, 1023–1035.
27 Y. Deng, J. Li, T. Qian, W. Guan and X. Wang, *J. Mater. Sci. Technol.*, 2017, **33**, 198–203.
28 X. Fu, Z. Liu, Y. Xiao, J. Wang and J. Lei, *Energy Build.*, 2015, **104**, 244–249.
29 Y. Konuklu and O. Ersoy, *Appl. Therm. Eng.*, 2016, **107**, 575–582.
30 M. Li, Z. Wu and H. Kao, *Appl. Energy*, 2011, **88**, 3125–3132.
31 S. Song, L. Dong, S. Chen, H. Xie and C. Xiong, *Energy Convers. Manage.*, 2014, **81**, 306–311.
32 S. Ramakrishnan, J. Sanjayan, X. Wang, M. Alam and J. Wilson, *Appl. Energy*, 2015, **157**, 85–94.
33 Z. Lu, J. Zhang, G. Sun, B. Xu, Z. Li and C. Gong, *Energy*, 2015, **82**, 43–53.
34 C. Li, B. Xie, D. Chen, J. Chen, W. Li, Z. Chen, S. W. Gibb and Y. Long, *Energy*, 2019, **166**, 246–255.

35 A. Karaipekli and A. Sarı, *Sol. Energy Mater. Sol. Cells*, 2016, **149**, 19–28.
36 D. Mei, B. Zhang, R. Liu, Y. Zhang and J. Liu, *Sol. Energy Mater. Sol. Cells*, 2011, **95**, 2772–2777.
37 A. Sarı, A. Karaipekli and C. Alkan, *Chem. Eng. J.*, 2009, **155**, 899–904.
38 C. Chen, X. Liu, W. Liu and M. Ma, *Sol. Energy Mater. Sol. Cells*, 2014, **127**, 14–20.
39 G. Ma, J. Sun, Y. Zhang, Y. Jing and Y. Jia, *Powder Technol.*, 2019, **342**, 131–140.